Detection of hydrosol inhomogeneities by polarization lidar

G.P. Kokhanenko, M.M. Krekova, I.E. Penner, and V.S. Shamanaev

Institute of Atmospheric Optics,
Siberian Branch of the Russian Academy of Sciences, Tomsk

Received April 26, 2004

By recording the polarization components of a lidar return signal one can significantly improve the efficiency of sensing of the upper ocean layer. The appearance of cross-polarized component of the lidar return is known to be related either to the presence of nonspherical particles in the scattering volume or to high level of multiple scattering. In natural waters both of these factors can work as the hydrosol particles are nonspherical and the optical depth of the water layer sounded can achieve significant values. As a result, the polarization pattern of the lidar return even in the surface layer is normally difficult to interpret. In this paper, an attempt to interpret data of polarization lidar measurements is made. It was aimed at detecting stratified structure of undersurface water. For this purpose, the results of numerical simulation of lidar returns are compared with the results of lidar observations. The scheme of formation of the cross-polarized component in the lidar return proposed explains the appearance of local depolarization maxima. Data of airborne lidar observations show that there exists a relation between variations of the extinction coefficient and the depolarization ratio along the flight line. It is shown that joint analysis of both of the polarization components of lidar returns yields higher quality of the information on hydrosol media.

Introduction

Laser sensing of water based on the effect of elastic scattering of light by hydrosol is an efficient method of investigation of the upper ocean layer and detection of underwater scattering layers and anomalies. The backscatter signals from hydrosol bear certain information about the spatial distribution of hydrooptical parameters, namely, on the extinction and backscattering coefficients. Despite some obvious difficulties caused by the influence of rough sea surface and the high level of multiple scattering,[1] the value of the average (over the sensing path) extinction coefficient can be retrieved from the experimental data quite reliably.[2,3] This in turn provides for the possibility of monitoring the variations of hydrooptical ocean parameters along the route of a vessel or an aircraft. However, the retrieval of the depth profile of optical parameters (extinction or backscattering) is really a challenge, and examples of successful retrieval are quite few in number.[4–6] Certainly, one of the difficulties is significant contribution of multiple scattering to a signal due to the high turbidity of the medium. The optical thickness τ of the surface water layer sounded to the depth of 10–30 m can achieve the values about 6 to 8, which is usually unattainable in the case of sensing along even extended atmospheric paths. A certain progress in solving this task is observed with the use of small-angle approximations.[7,8] However, from our point of view, the main factor preventing successful inversion of experimental data is the uncertainty in *a priori* set of the hydrosol scattering phase function.

The lidar equation in the single-scattering approximation

$$P(z) = Az^{-2}\beta_\pi(z)\exp\left[-2\int_0^z c(z')\mathrm{d}z'\right] \qquad (1)$$

formally includes two unknowns: the extinction coefficient $\tilde{n}$ and the backscattering coefficient $\beta_\pi \equiv \beta(180°)$. In its turn $\beta_\pi = \Lambda c g(180°)$, where $g(180°)$ is the backscattering phase function. The single scattering albedo $\Lambda = b/c$, where b is the scattering coefficient, is the parameter that depends on the absorptivity of the natural waters. The relation between the unknowns should be defined *a priori*, based on some model of the medium under study. In atmospheric investigations, the assumption of the constant value of the scattering phase function $g(180°)$ is usually fulfilled (in the first approximation). In this case, the backscattering coefficient β_π is proportional to the extinction coefficient and scattering layers of any nature are clearly seen in the backscattering signal. The situation for hydrosol is quite different. According to the commonly accepted model of formation of optical parameters of water,[9–11] the coefficient of directed scattering is determined by the three basic fractions: pure water itself (β_W), the fine, dominantly mineral fraction (β_S), and the fraction of large organic particles (β_L). As a result, the backscattering coefficient can be presented in the following form:

$$\beta_\pi = \beta_W(\pi) + \beta_S(\pi)\,C_S + \beta_L(\pi)\,C_L, \qquad (2)$$

where $\beta_W(\pi) = 2 \cdot 10^{-4}$ m$^{-1}\cdot$ sr^{-1} is the backscattering coefficient of water; C_S and C_L are the volume concentrations of the fine and coarse fractions, and the specific values of β_π for each fraction according to the model from Ref. 9 are: $\beta_S(\pi) = 8 \cdot 10^{-3}$ m$^{-1}\cdot$ sr^{-1} and

0235-6880/04/09 668-08 $02.00

$\beta_L(\pi) = 7 \cdot 10^{-5}$ m$^{-1} \cdot$ sr^{-1}. Despite the contributions of the fine and coarse fractions to the integral scattering coefficient $b = 2\pi \int_0^\pi \beta(\gamma) \sin\gamma \, d\gamma$ are quite comparable, backscattering is mostly determined by the fine fraction. It is natural to suppose that in the open-ocean water, far from river flows, inhomogeneous scattering layers are formed due to development of large organic particles. It is seen from Eq. (2) that the tenfold variation of C_L leads to only 10% variation of β_π. This not only complicates the solution of the inverse problem of sensing, because of inaccessible accuracy of the *a priori* setting of the scattering phase function, but can also lead to situation that scattering layers are indistinguishable in the backscattering signal.

For this reason, we have to use some *a priori* information, in addition to the intensity of the backscattering signal, in particular, the information about depolarization of the return signal. The currently available experimental and theoretical results do not provide for a comprehensive presentation of possible variations in the polarization pattern in sensing the natural waters.

In this paper, we attempt to interpret polarization lidar measurements in the problem on detecting stratification due to underwater inhomogeneities. For this purpose, the results of computer simulation of lidar signals are compared with the results of airborne lidar observations. The causes for an ambiguity in their interpretation are discussed.

1. Depolarization of return signals under conditions of prevalent multiple scattering (numerical simulation)

It is known that the appearance of cross-polarized component in the case of backscattering is caused either by scattering on nonspherical particles in the volume sounded or by high level of multiple scattering of radiation. In natural waters, both of these factors can work as the hydrosol particles are nonspherical and the optical depth of the water layer sounded can achieve significant values. The latter makes multiple scattering an important factor in the formation of the polarization pattern of return signal. The field experiments[12,13] do not allow us to distinguish between the contributions from these factors (multiple scattering or initial depolarization upon single backscattering) to the formation of the cross-polarized component of signals because of numerous uncertainties in the optical properties of the medium under study. In this respect, computer simulation (Monte Carlo technique) is very useful, because it provides for the possibility of estimating, with acceptable accuracy, the effect of optical parameters of the medium and the lidar geometry on the characteristics of return signals.

Assume that the initial radiation is linearly polarized and the Stokes vector of the initial radiation can be presented in the form $\mathbf{F}^0 = (1,1,0,0)$. The Stokes vector $\mathbf{F} = (I, Q, U, V)$ of radiation scattered in every light scattering event, can be presented in accordance with the equation

$$\mathbf{F}(\omega, r) = \mathbf{L}(\pi - \alpha_2)\mathbf{S}(\omega_j, \omega, r_j)\mathbf{L}(\alpha_1)\mathbf{F}(\omega_j, r_j), \quad (3)$$

where ω and ω_j are the radiation directions before and after the scattering event; $\mathbf{L}$ is the matrix of rotation; α_1 and α_2 are the angles between the scattering plane and the planes including the coordinate axes and the vectors ω_j and ω, respectively; $\mathbf{S}$ is the scattering phase matrix with the elements $S_{ik}(\omega_j, \omega, r_j) / S_{11}(\omega_j, \omega, r_j)$. A receiver detects the polarization components of the signal: parallel P_{co} and perpendicular P_{cros} to the direction of the initial polarization. The experimentally measurable depolarization ratio D, which is of interest for us, can be expressed through the components of the Stokes vector:

$$D = \frac{P_{cros}}{P_{co}} = \frac{I - Q}{I + Q}.$$

Algorithms of statistical modeling, which can be used to study the polarization characteristics of signals, are described in sufficient detail in Ref. 14 and therefore are not considered here. It should be only noted that for calculation of the lidar return, the scheme of local estimation of a flux was used[15] along with the modified modeling of trajectories with the preferred selection of the scattering direction toward the receiver with the corresponding change of the trajectory weight.[16]

The most important aspect in modeling is the selection of the adequate model for optical parameters of hydrosol. In our calculations, it is assumed that the hydrosol is a suspended matter consisting of two fractions: small mineral and large organic particles. The concentration ratio of these fractions C_S / C_L affects, first of all, the shape of the scattering phase function $g(\gamma)$. Based on the classification of hydrosol scattering properties proposed by Kopelevich,[9,17] we selected two experimentally measured scattering phase functions. The function with a pronounced forward directed peak $g_1(\gamma)$ (at $\langle\cos\gamma\rangle = 0.97$) is typical of the upper 100-m water layer of the open ocean, in which organic particles dominate; the function with the less pronounced peak $g_2(\gamma)$ was observed near river mouths with the increased content of particles of the mineral origin and for this function $\langle\cos\gamma\rangle = 0.91$. Apart from the scattering phase function, the behavior of other components of the scattering phase matrix in waters of different composition of the suspended matter is poorly studied now.

We used the scattering phase matrix[18] measured in the open ocean water as a typical one for particles of the organic fraction. For the mineral fraction, we had to use the Rayleigh matrix typical of molecular scattering. This is justified by the fact that small spherical terrigenic particles do not cause depolarization in the case of single backscattering, as well as in the case of molecular scattering.

First, let us consider the polarization characteristics of a signal from a homogeneous scattering layer for different values of the mixture ratio. This will allow

us to evaluate the effect of two factors on the total depolarization, namely, the initial depolarization and multiple scattering. The geometric parameters of the lidar (field of view $2\varphi = 8$ mrad, height above the surface 200 m) corresponded to the experiment described below in Section 3. Figure 1 shows the depolarization ratio as a function of depth for the medium with the content of the mineral fraction C_S / C_L = 0, 10, and 100%.

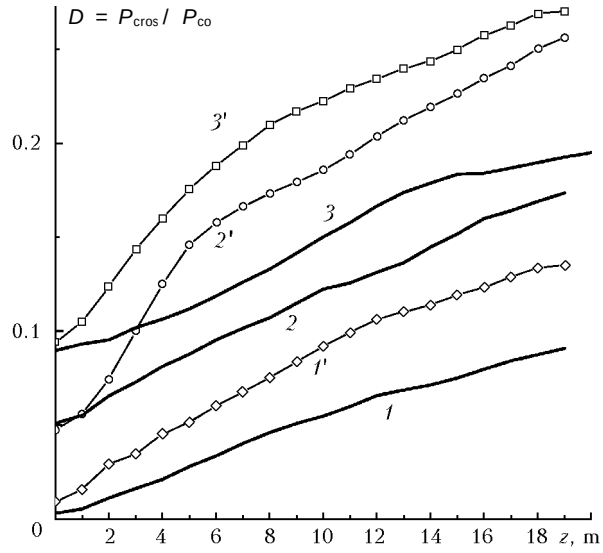

Fig. 1. Depth profiles of the depolarization ratio calculated for different values of the concentration ratio of mineral and organic particles; $\tilde{n} = 0.2$ m^{-1} (solid curves), $\tilde{n} = 0.4$ m^{-1} (squares); C_S = 100% (*1*, *1′*), 10% (*2*, *2′*), 0 (*3*, *3′*).

Two values of the extinction coefficient were taken: $\tilde{n} = 0.2$ m^{-1} (single scattering albedo $\Lambda = 0.75$, solid curves) and $\tilde{n} = 0.4$ m^{-1} ($\Lambda = 0.875$, squares). As would be expected, in the uppermost water layers (1–2 m), where the single scattering prevails, the depolarization ratio depends only on the composition of the mixture described by the values of the elements of the scattering phase matrix: $D = (S_{22} - S_{11}) / (S_{22} + S_{11})$ for the scattering angle of 180°. For the 100% content of organic fraction (curves *3*, *3′*) the initial depolarization is at the level $D \sim 0.08$. Even low (10%) content of the mineral fraction (*2*, *2′*) halves this value. With the increase of the depth, the role of multiple scattering increases, depolarization grows, and at the depth of 20 m the depolarization ratio is almost proportional to the optical thickness of the layer for the chosen composition of the mixture. At the depths of 5–15 m, which are of interest for laser sensing, there is no one-to-one correspondence between depolarization and the optical parameters of the medium. The signal coming from a more transparent medium, which includes only organic fraction ($\tilde{n} = 0.2$ m^{-1}, curve *3*), is depolarized stronger than that coming from a more turbid medium ($\tilde{n} = 0.4$ m^{-1}, curve *1′*), but including only the mineral fraction. However, as the part of the mineral fraction decreases to 10% (curve *2′*), depolarization becomes higher for the more turbid medium.

Thus, both of the factors under study play comparable roles in depolarization of the return signal. Taking into account that the depolarization increases most rapidly in the upper layers (2 to 3 m), which are usually inaccessible for processing because of the effect of the surface, it is impossible to determine, from the value of depolarization, whether it is caused by anisotropic particles or by multiple scattering.

2. Simulation of thin scattering layers

Consider now the peculiarities of detection of thin layers of enhanced turbidity. It was already mentioned above that the layers formed by large organic (or other anisotropic) particles are weakly pronounced in the signal intensity (component P_{co}), but can be clearly seen in depolarization. As an example, which formed the basis for the following computer simulation, let us consider the case of observation of the artificial inversion layer. The observations were carried out in March 2003 from the ice cover of Lake Baikal near Ivanovskii Cape. The distance from the lidar to the surface was 25 m. The receiver consisted of R7899 photomultipliers with the leading-edge time of 1.7 ns. The signal was digitized by a TDS3032Â oscilloscope with the step of 0.8 ns. Thus, real spatial resolution of the lidar was 0.2 m.

Photometer–transmissometer measurements[19] conducted simultaneously with lidar measurements showed that the homogeneous layer with the extinction coefficient $\tilde{n} = (0.25 \pm 0.01)$ m^{-1} was observed to the depth of 20 m. It should be noted that, according to the data of many-year observations, the transparency of water in this period was extremely high: the depth of Secchi disk visibility was 30–31 m, which corresponds to the ratio $Z_d = 7.2 / c$ characteristic of Baikal water.[20]

The inversion scattering layer was created using the suspended tooth paste (200 g per 10 liter water), consisting of particles of irregular shape with the size from few micrometers to 50 μm. This suspended matter was pumped into the water layer at the depth of 15 m. The lidar return signal (component P_{co}) from this layer is shown in Fig. 2*a* and the depolarization ratio is shown in Figs. 2*b* and *c* (these figures have different scales along the depth axis).

In the absence of the inversion layer, the signal intensity in the 2–20 m depth range decreased strictly in accordance with the exponential law with the deviations not exceeding the measurement error (10%). The extinction coefficient retrieved from the slope of the exponential decrease of the signal amounted to 0.17 m^{-1}.

The lower value of the extinction as compared to the contact measurements can be explained by the effect of multiple scattering because of a rather wide (8 mrad) lidar field of view.[1] In Fig. 2*a*, the polarized component $Đ_{co}$ of the signal in the presence of the inversion layer is shown by curve *1* with circles. Only a hardly noticeable plateau is present at the depth of 15–16 m, and then the signal returns to the initial exponential behavior. Within the framework of the

single scattering approximation (1), this is possible only in the case of negligibly small optical thickness of the additional scattering layer, including particles with somewhat higher backscattering β_π. However, the profile of the depolarization ratio exhibits a sharp peak at the same depth of 15–16 m (Figs. 2*a* and *b*), and in the deeper layers the depolarization again goes back to its initial value (~8%). Unfortunately, we do not know the depolarization ability of particles used for creation of the artificial scattering layer.

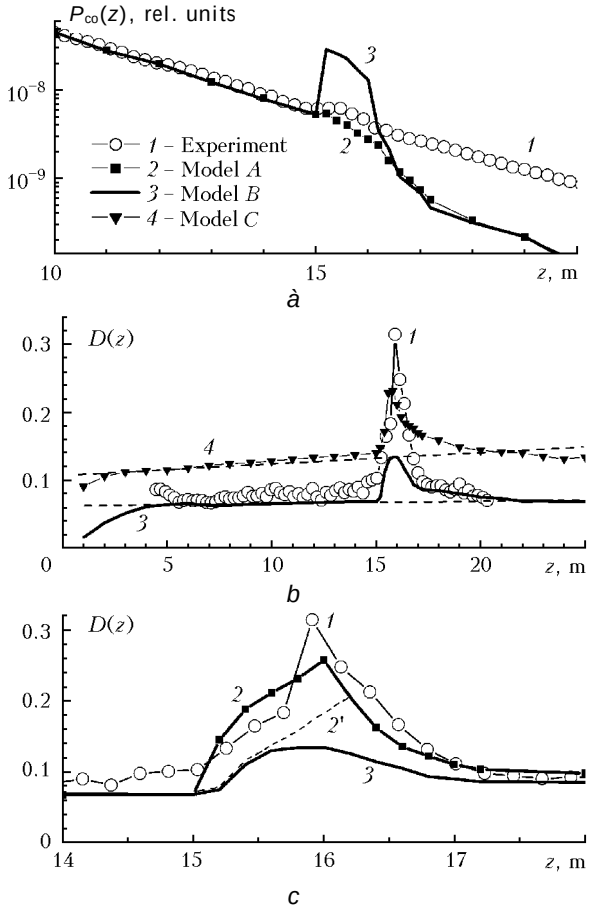

Fig. 2. Lidar returns from a thin scattering layer: experimental signal (*1*); calculations by models *A* (*2*), *B* (*3*), *C* (*4*).

Although the rigorous interpretation of these experimental results is impossible, we can clearly see high information content of the polarization sensing in the problem of detection of underwater inhomogeneities. In this case, the hydrosol in the inversion layer most likely produces higher, than outside the layer, depolarization in the single scattering, and this is in a good agreement with the behavior of the lidar signal. However, it remains unclear whether the layers of increased turbidity consisting of particles of the same kind as in the ambient medium can cause such peaks in the depolarization of the signal? In our opinion, this question remains open by now.

One of the points of view is based on the conclusions following from the small-angle approximation,[12,21,22] which is used quite successfully in describing lidar signals because of the pronounced forward peak of the scattering phase functions of hydrosol and high true absorption of radiation in water. Analysis of the small-angle scattering in disperse media[21,22] (as well as the radiation propagation in turbulent media[23]) usually involves the consideration of two depolarization mechanisms. The first one is the "geometric" mechanism, at which the direction of polarization turns due to the rotation of the electric vector around the ray in the case of nonplanar trajectory of propagation. The "diffraction" component of depolarization[24] is caused by that the components of the scattering phase matrix $S_{11}(\gamma)$ and $S_{22}(\gamma)$ in the forward direction ($\gamma \ll 1$) are unequal.

The typical solution obtained within the framework of this approximation by Vasilkov with co-authors[21] shows that the cross-polarized component of the signal, determined initially by the elements $S_{11}(\pi)$ and $S_{22}(\pi)$ of the scattering phase matrix, will then gradually and monotonically (which is very significant for this approximation) increase as the sensing point moves deeper into the water medium. The unique (for this medium) dependence of the increase rate of depolarization on the scattering coefficient allows the value of this coefficient to be retrieved from the polarization characteristics of the signal. Vasilkov, Goldin, and Gureev[12] have demonstrated the possibility of retrieving the profile of the scattering coefficient to the depth of 30 m. From the viewpoint of small-angle approximation only by the layers with the enhanced depolarization in single scattering can cause the peaks in depolarization.

Goldin with co-workers[13] observed near-bottom scattering layers formed, most likely, by homogeneous terrigenic particles and showed quite good agreement with this model. However, some results of statistical modeling[14] evidence the possibility of observing pronounced peaks in the depolarization of signals in the case of sensing turbid layers even with the depth-independent scattering matrix of hydrosol.

In this paper, we present an example of calculated polarization components of a lidar signal from a thin scattering layer, which demonstrates this effect to be realistic in principle.

The scheme of calculation corresponded to the experiment on observation of an artificial inversion layer. A 1-m thick inversion layer with the enhanced turbidity is located at the depth of 15 m. The sensing is performed with a lidar having the field of view $2\varphi = 8$ mrad located at 25 m from the water surface. Several models of the inversion layer were considered. In model *A*, it is assumed that the mineral fraction with the scattering phase function $g_2(\gamma)$ is present in the most part of water. The scattering coefficient is $b = 0.16$ m^{-1}, and in this case the backscattering coefficient is $\beta_\pi = 0.0014$ m^{-1}/sr. The inversion layer is formed by the hydrosol of the coarse organic fraction [scattering phase function $g_1(\gamma)$] with the backscattering coefficient β_π, exceeding the background value by 15%: $\beta_\pi = 0.0016$ m^{-1}/sr, corresponding to $b = 1.2$ m^{-1}. Thus, model *A* corresponds to the case of

a very turbid scattering layer, which is hardly seen in the backscatter because of the change in the shape of the scattering phase function.

In models *B* and *C*, the scattering coefficients are the same as in model *A* (b_1 = 0.16 m^{-1}, b_2 = 1.2 m^{-1}), but the qualitative composition of hydrosol is constant with the depth: it is represented by the mineral fraction for model *B* (scattering phase function g_2 and the Rayleigh scattering phase matrix) and by the organic fraction for model *C* (scattering phase function g_1 and scattering phase matrix from Ref. 18).

The behavior of the intensity of the signals calculated (component $Ð_{co}$) is quite predictable. For model *B* (curve *3* in Fig. 2*a*), the marked peak in the intensity at the layer boundary (proportional to the increase of β_π) is observed. For model *A*, in which the value of β_π in the layer is only 15% higher, a hardly noticeable spike and only the faster descent of the intensity in the layer following the law $\exp(-2cz)$ are observed. The behavior of the experimental signal better resembles that by the model *A*, but the lower underestimation of the intensity after the passage though the layer is indicative of the much smaller optical thickness of the artificial layer.

Figures 2*b* and *c*, on different scales, compare the profiles of the depolarization ratio for the experimental lidar signal (curve *1*) and three model calculations. It is seen from Fig. 2*b* that in the upper layers (0–5 m) for models *B* (mineral fraction, curve *3*) and *C* (organic fraction, curve *4*) the depolarization increases quickly, and then the increase becomes slower and closer to the linear one. The increase rate of the depolarization is higher for the organic fraction. As to the depolarization ratio, the experimental signal is closer to that calculated for the mineral fraction. In the region of location of the inversion layer, a peak of depolarization is observed for all the models, even if the scattering phase matrix is constant all over the layer. The profile of depolarization of the experimental lidar signal inside the layer (see Fig. 2*c*) is close to that calculated by the model *À* (curve *2*, depolarizing layer).

The excess of depolarization for model *A* over the initial depolarization at single scattering inside the layer (D = 0.0748) is shown by the dashed curve *2′* and it is higher than the depolarization for the model *B*. This is likely explained by a more pronounced forward peak in the scattering phase function of large organic particles. With the further increase of the depth, the depolarization for all the models decreases gradually and goes back to the level, it had in the homogeneous medium (this level is shown by the dashed straight lines.) The total gradient of depolarization (related to the extinction coefficient) $\delta = \frac{1}{c}\frac{\mathrm{d}D}{\mathrm{d}z}$ is 0.0014 for the mineral fraction and 0.01 for the organic fraction in the upper layers. The latter is close to the value determined experimentally in Ref. 12 (δ = 0.009).

The origin of local depolarization peaks in the scattering layers becomes clear, if one accepts that the depolarization is determined not only by the small-angle scattering, but also by multiple scattering (in particular, to large angles) inside the layers with enhanced turbidity. Since the direction of the scattering plane changes in a random way in the successive scattering events, [according to Eq. (1)] the photon polarization changes too. Finally, the photon, coming back to the receiver field of view, remains polarized, but the direction of preferred polarization is random for each of the photons. The scattering by suspended particles is incoherent, which results in the appearance of the nonzero depolarized component in the signal. The value of the cross-polarized component (after reduction to the initial reference plane) depends on the angle (angles) of photon scattering during the propagation. The scattering to large angles implies significantly higher depolarization than in the case of small-angle scattering.

It is known[25] quite well that a part of the multiply scattered radiation comprising the signal is proportional to the optical diameter η of the spot formed by the lidar field of view (2φ) at the place of location of the scattering layer (approximately, $\eta = 2b\varphi z$, where z is the distance to the scattering point). The photons leaving the field-of-view cone upon the first scattering event have negligibly low probability to come back into the receiver field of view, because it is small. The probability that the photon remains within the lidar field of view in the case of scattering to large angles is determined as $p = 1 - \exp(-\tilde{n}\varphi z) \approx \eta$ at $\eta << 1$. Therefore, the value of the "local" depolarization (which is determined just by the scattering to large angles) in our case also proves to be proportional to the optical diameter η. After the beam propagates through a turbid scattering layer, the value of η decreases sharply, thus leading to the gradual decrease of depolarization and its return to the initial profile.

Thus, the results presented allow us to propose the cross-polarized component of the signal to be a sum of three terms (the scheme is shown in Fig. 3; the inversion layer lies at the depth z_1–z_2):

$$D_\Sigma(z) = D_1\left(\frac{S_{22}(\pi)}{S_{11}(\pi)}\right) + D_2\left[b(z), g(\gamma), 2\varphi\right] + D_3\left[\tau, g(\gamma), 2\varphi\right]. \quad (4)$$

In Eq. (4), D_1 (curve *1* in Fig. 3) presents the cross-polarized component arising at single backscattering and by the values of the elements $S_{11}(\pi)$ and $S_{22}(\pi)$ of the scattering phase matrix. In rarefied media (aerosol), it is the dominant component, but in water, it manifests itself only in the case of a sharp change in the type of scattering particles.

The parameter D_2 presents the radiation depolarization due to multiple scattering to large angles in the layer with enhanced turbidity determined by high value of the scattering coefficient of the medium, the receiver field of view 2φ, and the scattering phase function. Photons scattered to large angles in the regions with enhanced scattering acquire an additional mean free path and thus can reach the receiver at the time corresponding to the spatial zone

behind the layer boundary. In contrast to the single-scattering signal, the multiple-scattering signal does not decrease sharply outside the layer. Quite similar behavior of depolarization – the smooth decrease outside the layer (see Fig. 2*c*) – allows us to suppose that this cause prevails in observing layers of enhanced turbidity.

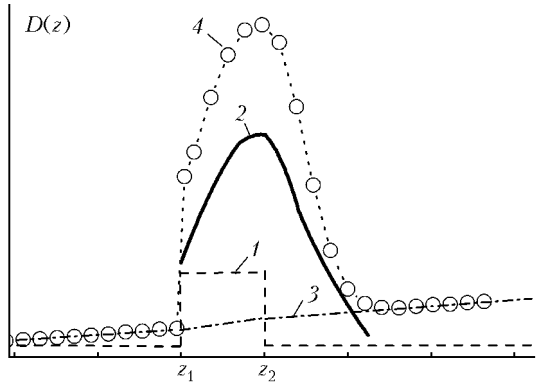

Fig. 3. Scheme of formation of the cross-polarized component of the lidar signal: depolarization components by Eq. (4) (*1, 2, 3*) and total depolarization (*4*).

Finally, D_3 describes the monotonic increase of depolarization, determined by the integral optical thickness of the layer $\tau = bz$ and caused by multiple scattering to small angles. At a small lidar field of view (for our lidar, 8 mrad in air or 6 mrad in water), the slow increase of depolarization will be masked by any significant changes in the optical parameters of hydrosol, and it is hardly possible to unambiguously retrieve the profile of extinction from the gradient of the depolarization ratio.

Curve *4* in Fig. 3 presents the total depolarization D_Σ. Equation (4) cannot be considered exact, because, actually, the components D_2 and D_3 themselves depend on the components of the scattering phase matrix S_{ij} and cannot be distinguished quite accurately. However, noticeable effect of the local component of depolarization D_2, as an addition to the monotonically increasing background, allows us to consider it as complementary component that enables us to use the peculiarities of depolarization for identification of scattering layers.

3. Experimental observations of hydrooptical inhomogeneities by airborne lidar

A certain idea on the mutual variations of the extinction coefficient and depolarization of the backscattered radiation in natural waters can be gained from the results of observation of seawater by use of an airborne lidar. The depolarization of lidar signals was observed in November 1996 over Lake Baikal[26] and in June 1997 near the coast of Scotland.[27] In both of these cases, the sensing was carried out from onboard an aircraft flying at the altitude of 200 m above the water surface. The lidar had a telescope of 150 mm in diameter and a Nd:YAG laser emitting pulses of 50 mJ energy at the wavelength of 0.53 μm, at a pulse repetition frequency of 5 Hz. The field of view was $2\varphi = 8$ mrad. To digitize the recorded lidar return signal, we used a 7-bit analog-to-digital converter (ADC) with the discretization step of 8 ns and the band of 33 MHz (this corresponds to the real depth resolution of 3 m). The received optical signal was split by the Wollaston prism into two polarization components: the component parallel to the polarization P_{co} of sounding radiation and the perpendicular one, P_{cros}. Each of the signals was recorded with an individual PMT. Unfortunately, we failed to carry out absolute calibration of the channels, and the depolarization ratios $D = P_{cros} / P_{co}$ presented here are known accurate to a constant factor. The measurement errors in the signal power, at the center of the receiver working range, amount to 12–15% in sensing only slightly turbid water ($\tilde{n} = 0.12$ m^{-1}) and increase to 18–20% in turbid water ($\tilde{n} = 0.36$ m^{-1}) because of the higher rate of signal variation at the ADC input. As a result, the relative error in determination of depolarization at any point of the signal can achieve 25%.

Figure 4 (see the inset) depicts the examples of lidar records obtained at flight parts with pronounced spatial inhomogeneities in the optical parameters of the water. The upper plots show the variation of the extinction coefficient along the flight line. The direction of the flight is from left to right, and the flight distance L is plotted as an abscissa.

The extinction coefficient $\tilde{n}$, averaged over the depth range of 5–15 m, was estimated from the signal fall off rate on the logarithmic scale assuming homogeneous water. This assumption is based on that the deviations of the recorded signal from the exponential fall off nowhere exceed digitizing errors. It should be taken into account that at the 8-mrad field of view, used in our lidar, the retrieved extinction can be somewhat underestimated (to 30%) due to the contribution from multiple scattering.[1]

The lower panels in Figs. 4*a–c* show two-dimensional (depth z – distance L) map of depolarization of the D-signal drawn in colors. The depths smaller than 5 m are omitted, because the signals from them exceed the digitization range. The maximum depth is limited to the range, where the values in one of the channels become smaller than 2 bits of the ADC. The depth profiles of the depolarization ratio at the most interesting points of the flight (figures in white circles) are shown in the right panel of Fig. 4.

Figure 4*a* depicts the record of the flight over Lake Baikal along the direction toward the Selenga River mouth. In this region of the lake, high turbidity of water is determined by the inflow of large amount of small mineral particles (clay) with the river water. This fine suspended matter may not cause the depolarization in single scattering, and it should be expected that the signal depolarization in this case is caused by multiple scattering. Indeed, we can

see that the variations of depolarization fully correlate with the variations of the extinction coefficient along the flight line. The gradient of depolarization d*D* / d*z* is higher for point *3* (more turbid water). Note that the sharp increase of depolarization at the depth of 14 m at point *4* corresponds to the reflection from the lake bottom, whereas in the polarized component the signal from the bottom becomes noticeable from the 10-m depth.

Figure 4*b* corresponds to the northeast flight from the coast of Scotland into the open sea. The sharp decrease of the water turbidity a minute later from the beginning of the flight corresponds to the transition from the coastal water enriched with terrigenic particles to the more transparent water of the open ocean. The proportional decrease of depolarization agrees with this assumption. At a distance of 20 km, an insignificant increase of the extinction, only slightly exceeding the measurement errors, is observed. However, the depolarization ratio in this region increases sharply, far exceeding the level of depolarization in the turbid coastal waters. Certainly, this is caused by the increase in the relative content of the large organic fraction (phyto- and zooplankton), causing depolarization in single scattering because of the nonspherical shape of the organic particles. The depth-averaged depolarization gradient here (point *3*) is also higher than at point *1*, which is explained by a more pronounced peak of the scattering phase function for organic particles and, consequently, by higher contribution of multiple scattering.

The characteristic case of the unmatched variation of the depolarization and extinction along the flight line is shown in Fig. 4*c*. This figure shows the flight over a part of the North Atlantic Current between the Shetland and Faeroe Islands. An area with more turbid water (about 5 km across) is characterized by the significant increase of depolarization. It is interesting to note that here the peak of depolarization (point *2*) is markedly shifted with respect to the peak of turbidity (point *3*) in the direction of the frontal zone. It is quite probable that just the frontal zone is the place of maximum development of large nonspherical bioplankton particles, whereas in somewhat more turbid water (to the right from point *3*) small nonspherical particles make up a large fraction. In addition, one can clearly see here that the gradient of depolarization is mostly determined by the type of the scattering particles (that is, the components of the scattering phase matrix), rather than by the absolute value of the extinction coefficient.

Unfortunately, the absence of any *a priori* information about the scattering phase matrix of the suspended matter, as well as the reliable models of hydrosol polarization characteristics, does not allow us to retrieve the quantitative information about the optical parameters of the medium from the observations of depolarization in the general case. We can speak only about the qualitative interpretation of the observations. Thus, at the constant extinction coefficient, the sharp variations of depolarization are indicative of the variations in the content of large organic particles. The variations of depolarization are fully caused by the corresponding variations only of the extinction in the case of prevalence of the fine mineral fraction, for example, when observing nepheloid layers near the bottom or near the river mouths. The nonsynchronous behavior of the depolarization and the extinction coefficient is indicative of the change in the ratio between the coarse (organic) and fine hydrosol fractions. This is also true for the depth profiles – inhomogeneities in polarization are most likely caused by the changes in the scattering phase matrix of the medium, and the depolarization gradient is determined by the components of the matrix, due to which the one-to-one correspondence between the degree of depolarization and the extinction coefficient hardly exists.

It is characteristic that we quite frequently observed inhomogeneities similar to those shown in Fig. 4*c* (there are six similar records recorded during 30 flight hours over the coastal waters of Scotland). At the same time, only once we observed the situation with the significant deviation of the signal intensity fall off from the exponential law.[4] This situation permitted us to reveal vertical inhomogeneities in the extinction coefficient through the inversion of Eq. (1). This case again emphasizes high information content of the polarization lidar sensing of hydrosols.

Conclusions

The polarization lidar sensing provides for obtaining additional information on the optical properties of the hydrosol. This concerns, in the first turn, the possibility of detecting inversion scattering layers both in the water depth and near the bottom. This is especially significant in the surface layers, because the variation of the concentration of large organic particles weakly affects the value of the backscattering coefficient β_π and, therefore, only slightly manifests itself in the lidar signal. The variations of the contribution of different hydrosol fractions (fine mineral and coarse organic ones) result in the change of the depolarization ratio at single backscattering and, thus, they are clearly seen in the cross-polarized signal. However, the high level of multiply scattered radiation leads to ambiguities in the data interpretation. The calculations show that the inversion layers formed both by the increased concentration of the background hydrosol and by nonspherical particles give rise to similar local peaks in the depolarization profile.

The optical parameters of natural water (pronounced forward peak of the scattering phase function, significant absorption) favor the formation of the light field intensity mostly by the small-angle scattering and, therefore, are satisfactorily described by the small-angle approximation. However, a part of radiation is scattered to large angles and forms the diffuse background, which is depolarized to a significant extent already at the small optical thickness.[28] The contribution of this background to the total radiation intensity is insignificant, but its role is decisive in

formation of the cross-polarized component of the signal from the place, where the layer with the enhanced turbidity is located. The radiation underwent the scattering to large angles quickly leaves the lidar field of view, which explains the decrease in the degree of depolarization after passage through the layer.

Unfortunately, with only one reliably measured scattering phase matrix,[18] now it is impossible to speak about the accurate statistical modeling of the process of radiation depolarization in water and its connection with the composition of the suspended matter. To all appearance, the unambiguous retrieval of the profile of scattering coefficient from observations of only depolarization is hardly possible. The joint analysis of both of the polarized and cross-polarized components of the lidar signal allows obtaining more reliable information about the hydrosol medium.

Acknowledgments

The authors are grateful to V.V. Veretennikov and G.M. Krekov for valuable criticism and participation in discussion of the results.

This work was supported, in part, by CRDF, project No. RG2–2357–TO–02.

References

1. G.P. Kokhanenko, M.M. Krekova, I.E. Penner, and V.S. Shamanaev, Atmos. Oceanic Opt. **13**, No. 4, 337–346 (2000).
2. J.H. Churnside, V.I. Tatarskii, and J.J. Wilson, Appl. Opt. **37**, No. 15, 3105–3112 (1998).
3. G.P. Kokhanenko, I.E. Penner, and V.S. Shamanaev, Atmos. Oceanic Opt. **11**, No. 7, 614–620 (1998).
4. V.V. Veretennikov, G.P. Kokhanenko, and V.S. Shamanaev, in: *Advances in Laser Remote Sensing. Selected Papers of 20th ILRC* (Vichy, France, 2000), pp. 145–148.
5. O.A. Bukin, V.I. Il'ichev, A.Yu. Maior, A.N. Pavlov, A.G. Stafievskii, and V.A. Tyankin, Atmos. Oceanic Opt. **7**, No. 10, 761–763 (1994).
6. B. Billard, R.H. Abbot, and M.F. Penny, Appl. Opt. **25**, No. 13, 2080–2088 (1986).
7. V.V. Veretennikov, Proc. SPIE **3983**, 260–270 (1999).
8. E.P. Zege and L.I. Chaikovskaya, Izv. Akad. Nauk SSSR, Fiz. Atmos. Okeana **21**, No. 10, 93–96 (1985).
9. O.V. Kopelevich, in: *Ocean Optics*. Vol. 1. *Physical Ocean Optics* (Nauka, Moscow, 1983), pp. 208–235.
10. K.S. Shifrin, *Introduction to Ocean Optics* (Gidrometeoizdat, Leningrad, 1983), 278 pp.
11. N.G. Jerlov, *Optical Oceanography* (Elsevier Publishing Co., New York, 1968), 194 pp.
12. A.P. Vasilkov, Yu.A. Goldin, and B.A. Gureev, Izv. Ros. Akad. Nauk, Fiz. Atmos. Okeana **33**, No. 4, 563–569 (1997).
13. Yu.A. Goldin, A.P. Vasilkov, B.A. Gureev, F.E. Hoge, R.N. Swift, and C.W. Wright, in: *Current Problems in Optics of Natural Waters. Proc. of D.S. Rozhdestvensky Optical Society* (St. Petersburg, 2001), pp. 127–132.
14. G.M. Krekov, M.M. Krekova, and V.S. Shamanaev, Appl. Opt. **37**, No. 9, 1596–1601 (1998).
15. G.I. Marchuk, ed., *Monte Carlo Technique in Atmospheric Optics* (Nauka, Novosibirsk, 1976), 284 pp.
16. V.V. Belov, G.M. Krekov, and G.A. Titov, in: *Some Issues of Remote Atmospheric Sensing*, ed. by V.E. Zuev (IAO SB AS USSR, Tomsk, 1975), pp. 102–116.
17. O.V. Kopelevich, "*Optical Properties of Seawater*," Doct. Tech. Sci. Dissert. (1987).
18. K.J. Voss and E.S. Fry, Appl. Opt. **24**, No. 23, 4427–4439 (1984).
19. P.P. Sherstyankin, G.P. Kokhanenko, I.E. Penner, A.P. Rostov, L.N. Kuimova, V.G. Ivanov, and V.V. Blinov, Dokl. Ros. Akad. Nauk, Geofiz. **383**, No. 1, 106–110 (2002).
20. P.P. Sherstyankin, in: *Physical Limnology of Lake Baikal: a Review*, ed. by M.N. Shimaraev and S. Okuda (Baikal International Center for Ecological Research, Irkutsk–Okayama, 1994), pp. 24–30.
21. A.P. Vasilkov, T.V. Kondranin, and E.V. Myasnikov, Izv. Akad. Nauk SSSR, Fiz. Atmos. Okeana **24**, No. 8, 873–882 (1988).
22. E.E. Gorodnichev, A.I. Kuzovlev, and D.B. Rogozkin, Izv. Ros. Akad. Nauk, Fiz. Atmos. Okeana **19**, No. 3, 371–383 (2003).
23. Yu.A. Kravtsov, Izv. Vyssh. Uchebn. Zaved., Radiofiz. **13**, No. 2, 281–285 (1970).
24. V.I. Tatarskii, Izv. Vyssh. Uchebn. Zaved., Radiofiz. **10**, No. 12, 1762–1763 (1967).
25. G.M. Krekov and M.M. Krekova, Atm. Opt. **2**, No. 1, 55–61 (1989).
26. G.P. Kokhanenko, I.E. Penner, V.S. Shamanaev, G. Ladbrook, and A. Scott, Atmos. Oceanic Opt. **12**, No. 1, 37–43 (1999).
27. G.P. Kokhanenko, I.E. Penner, and V.S. Shamanaev, Atmos. Oceanic Opt. **14**, No. 12, 1038–1042 (2001).
28. V.V. Vergun, E.V. Genin, G.P. Kokhanenko, V.A. Krutikov, and D.S. Mezhevoi, Atm. Opt. **3**, No. 7, 631–637 (1990).

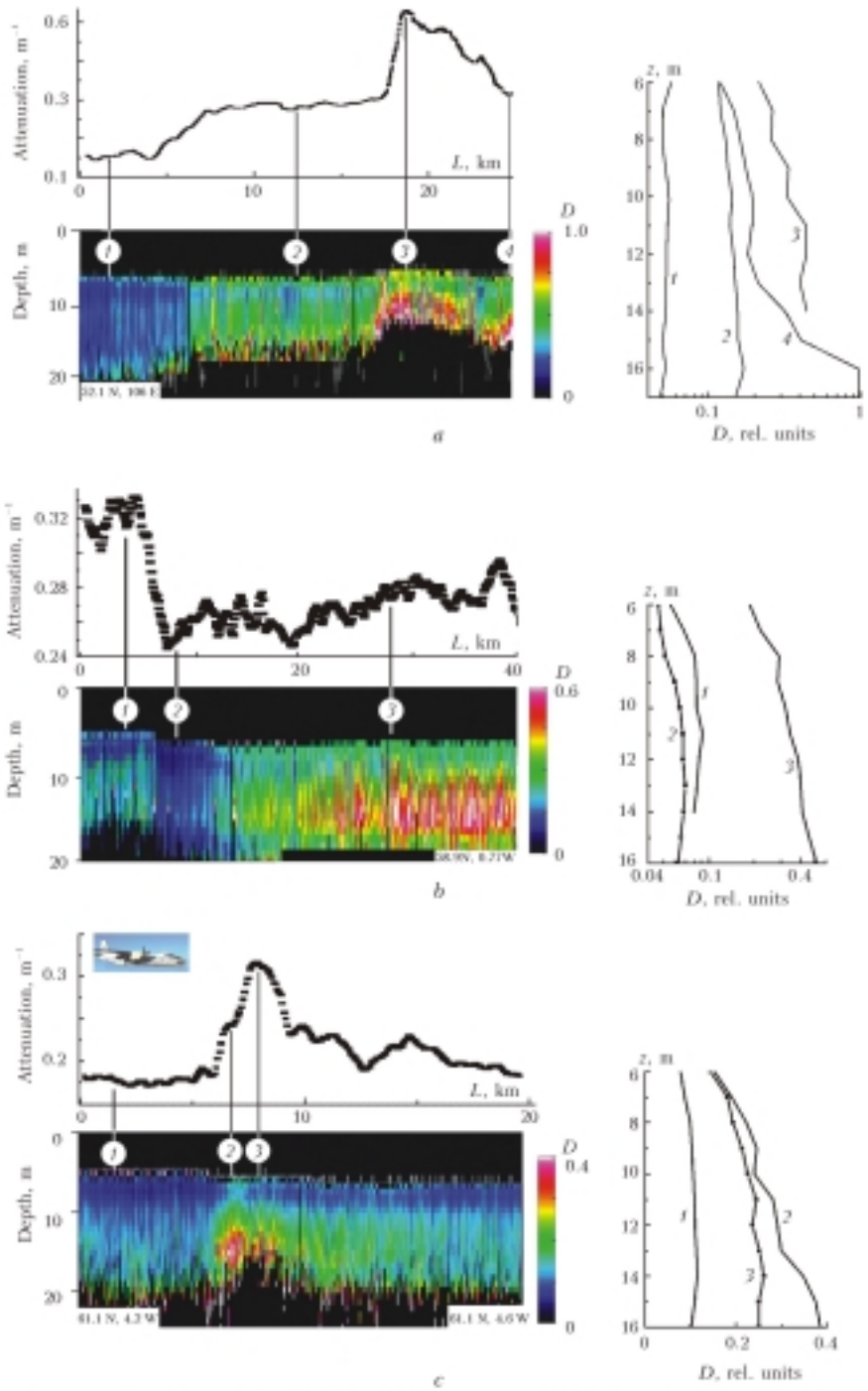

Fig. 4. Airborne observations of depolarization of lidar signals: Lake Baikal, November 1996 (*a*); the North Sea, June 1997 (*b*); the Norway Sea, June 1997 (*c*).